Protecting Quantum Information via Destructive Interference of Correlated Noise

Alon Salhov,[1,*,§] Qingyun Cao,[2,3,§] Jianming Cai,[3,†] Alex Retzker,[1,4] Fedor Jelezko,[2] and Genko Genov[2,‡]
[1]Racah Institute of Physics, The Hebrew University of Jerusalem, Jerusalem, 91904, Givat Ram, Israel
[2]Institute for Quantum Optics, Ulm University, Albert-Einstein-Allee 11, 89081 Ulm, Germany
[3]School of Physics, International Joint Laboratory on Quantum Sensing and Quantum Metrology, Huazhong University of Science and Technology, Wuhan 430074, China
[4]AWS Center for Quantum Computing, Pasadena, California 91125, USA

(Received 27 November 2023; accepted 8 April 2024; published 30 May 2024)

Decoherence and imperfect control are crucial challenges for quantum technologies. Common protection strategies rely on noise temporal autocorrelation, which is not optimal if other correlations are present. We develop and demonstrate experimentally a strategy that uses the cross-correlation of two noise sources. Utilizing destructive interference of cross-correlated noise extends the coherence time tenfold, improves control fidelity, and surpasses the state-of-the-art sensitivity for high frequency quantum sensing, significantly expanding the applicability of noise protection strategies.

DOI: 10.1103/PhysRevLett.132.223601

Introduction.—Decoherence, typically caused by unwanted couplings to the environment and control noise [1,2], remains a major challenge for quantum technologies. Quantum computation requires reducing its effect to achieve the long memory time and high gate fidelity required for fault tolerance [3,4]. The sensitivity of quantum sensors typically scales with the sensor's coherence time and is thus also limited by decoherence [5]. While fabrication efforts focus on minimizing noise in quantum devices [6] and quantum error correction techniques allow detection and correction of noise-induced errors [7,8], several important strategies, such as decoherence-free spaces [9], clock transitions [10], dynamical decoupling [11], and composite pulses [12–19], reduce the effect of noise, lowering decoherence and control error rates [20].

Each strategy takes advantage of a "resource" to protect quantum information. Decoherence-free subspaces, for example, employ symmetries in system-bath coupling by storing quantum information in subspaces with low noise susceptibility. Temporal autocorrelations of noise constitute another resource, which dynamical decoupling and composite pulses utilize to partially refocus the effect of system-environment interactions and control noise.

In this work, we propose and experimentally demonstrate a protection strategy that relies on a different kind of resource—the cross-correlation of two noise sources, e.g., control fields. Such cross-correlations exist when the control fields are generated from the same source or pass through the same transmission line. As an example, we modify the concatenated continuous dynamical decoupling control scheme [21], which has been experimentally demonstrated for coherence protection and quantum sensing [22–32]. As we show, introducing a frequency shift to one of the control fields, which is proportional to the degree of cross-correlation, results in destructive interference of the cross-correlated noise. Our scheme gives an order-of-magnitude enhancement of coherence time, compared to the standard technique, and is limited mainly by the lifetime of the qubit. We use it for improved quantum sensing and robust qubit operations, demonstrating its advantages and broad applicability. Beyond concatenated decoupling, utilizing noise correlations can also be beneficial for other systems and experimental protocols, e.g., for optimization of refocusing pulses and robust coherent control of two- and three-state quantum systems [33].

Theory.—We consider a two-level system with a Hamiltonian ($\hbar = 1$)

$$H = \frac{1}{2}[\omega_0 + \delta(t)]\sigma_z + \Omega_1[1 + \epsilon_1(t)]\cos(\omega_0 t)\sigma_x - 2\Omega_2[1 + \epsilon_2(t)]\sin(\omega_0 t)\cos(\widetilde{\Omega}_1 t)\sigma_x, \quad (1)$$

where ω_0 is the qubit bare energy gap, $\delta(t)$ is an environment-induced noise term, Ω_1 is the Rabi frequency of a protective field, perpendicular to the noise [21], with $\epsilon_1(t)$ its relative error [33]. We compensate the first field noise by a second field with Rabi frequency Ω_2, modulation frequency $\widetilde{\Omega}_1$, and relative error $\epsilon_2(t)$. The noise terms are assumed stationary with equal, subunity variance $[\overline{\epsilon_i(t)} = 0, \sigma^2 \equiv \overline{\epsilon_i(t)^2} \ll 1$; overbar indicates average over

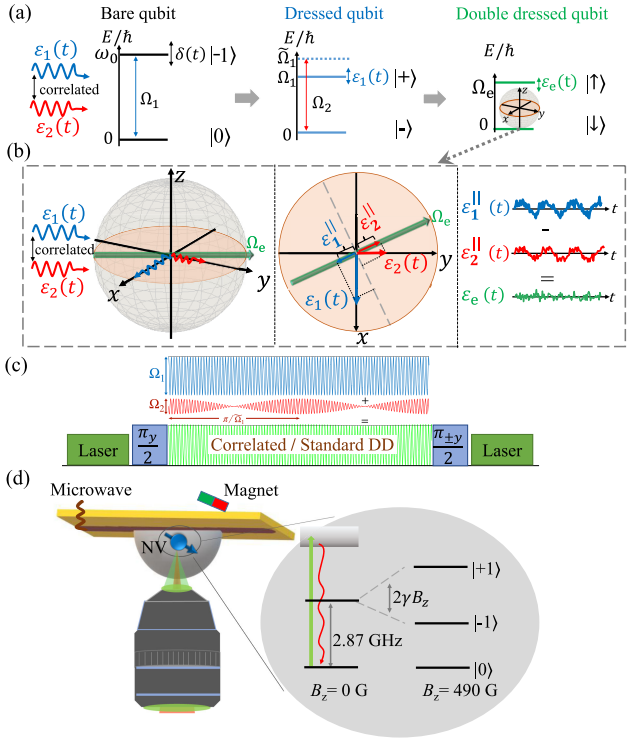

FIG. 1. Schematic representation of destructive interference of cross-correlated noise, control sequences, and experimental setup. (a) The qubit is subjected to environmental noise $\delta(t)$. Applying a resonant drive with Rabi frequency Ω_1 creates a protected dressed qubit which decoheres mainly due to $\epsilon_1(t)$—the noise in Ω_1. Applying a second drive with modulation frequency $\widetilde{\Omega}_1$, Rabi frequency Ω_2, and noise $\epsilon_2(t)$ reduces decoherence due to $\epsilon_1(t)$. (b) If the cross-correlation c of $\epsilon_1(t)$ and $\epsilon_2(t)$ is nonzero, a detuning $\widetilde{\Omega}_1 - \Omega_1 = c\Omega_2^2/\Omega_1$ tilts the effective-drive axis and induces a destructive interference of the cross-correlated noise, resulting in a doubly dressed qubit with a longer coherence time. (c) Measurement sequences for standard and correlated double drive (DD). The only difference is the value of the modulation frequency of the second driving field $\widetilde{\Omega}_1$, which is Ω_1 for standard DD and according to Eq. (3) for correlated DD. The two fields are generated using the same channel of an arbitrary waveform generator and combined into one waveform. (d) Experimental setup and level scheme of the NV center.

experimental runs]. The equal variance assumption is experimentally motivated [33,57], but can be relaxed.

The standard double drive [21,22] relies on the mechanism of continuous dynamical decoupling [see Fig. 1(a) and [33]]. We abbreviate double drive to DD further on (not to be confused with dynamical decoupling). Disregarding potential cross-correlations, the noise of the first field $\epsilon_1(t)$ is optimally decoupled at the standard resonance condition $\widetilde{\Omega}_1 = \Omega_1$, but the system suffers from the second field noise $\epsilon_2(t)$ [21,22,33].

Detuning $\widetilde{\Omega}_1$ from resonance reintroduces the effect of $\epsilon_1(t)$ when there is no cross-correlation between the noise terms, i.e., $\overline{\epsilon_1(t)\epsilon_2(t)} = 0$. However, nonzero cross-correlations are expected when the fields share control hardware. Then, reintroduction of $\epsilon_1(t)$ is beneficial, if it is set to destructively interfere with $\epsilon_2(t)$. To show this, we transform H into a doubly rotating frame at $\omega_0\sigma_z/2$ and then $\widetilde{\Omega}_1\sigma_x/2$, and apply the rotating-wave approximation $\Omega_2 \ll \Omega_1, \widetilde{\Omega}_1 \ll \omega_0$ to obtain [33]

$$H_{\mathrm{II}} = \frac{(\Omega_1 - \widetilde{\Omega}_1) + \Omega_1\epsilon_1(t)}{2}\sigma_x + \frac{\Omega_2}{2}[1 + \epsilon_2(t)]\sigma_y. \quad (2)$$

To prolong the doubly dressed [58] qubit's coherence time, we choose $\widetilde{\Omega}_1$ to minimize the variance of its energy gap. The resulting detuning $(\widetilde{\Omega}_1 - \Omega_1)$ tilts the effective-drive axis to a correlation-dependent angle. Then, the projections of the correlated noise terms on this axis, which affect decoherence to first order, destructively interfere [see Fig. 1(b) and [33] for analysis and further discussion on cross-spectral densities]. The optimal modulation frequency of the second drive, to leading order in $\Omega_2 \ll \Omega_1$, reads

$$\widetilde{\Omega}_1 \approx \Omega_1 + c\frac{\Omega_2^2}{\Omega_1}, \quad \text{where } c \equiv \frac{\overline{\epsilon_1(t)\epsilon_2(t)}}{\sigma^2} \quad (3)$$

is the cross-correlation of the fields' fluctuations. Note that this correlation-induced frequency shift is not related to the Bloch-Siegert shift $(\Omega_2^2/4\Omega_1)$ [59,60]. It has a different magnitude and physical origin and exists with circularly polarized control fields, where the latter is zero because there are no counter-rotating terms. A complete treatment of both effects requires substituting $c \to (c + \frac{1}{4})$ into Eq. (3) [33].

The *correlated noise shift* in Eq. (3) [with the $c \to (c + \frac{1}{4})$ correction] is the main result of this section and defines the correlated DD protocol. Typically, c is system dependent, suggesting to scan the detuning and optimize the coherence time [33]. By doing so, we observe an almost perfect correlation ($c \approx 1$) in our experimental setup, which allows complete noise suppression to first order as the doubly dressed states become (dynamic) clock states [33] (see Supplemental Material Eq. S.15 for coherence time analysis). The resulting stability of the dressed qubit is better than simply the stability of its components, that is, the bare qubit or the control. As Eq. (3) reduces to the standard DD for $c = 0$ we conclude that the destructive interference principle is compatible with dynamical decoupling. We distinguish the contribution of the two-field cross-correlation from the standard DD effect by comparing the two protocols. In the following, we demonstrate the superiority of correlated DD for (1) quantum memory, (2) quantum sensing, and (3) robust coherent control.

Quantum memory.—We experimentally demonstrate correlated DD for a quantum memory in a single nitrogen-vacancy (NV) center in diamond. The diamond sample is

produced by chemical vapor deposition (CVD) and polished into a hemisphere, acting as a solid immersion lens and enhancing photon collection efficiency [33,61,62]. To create NV centers, the surface is overgrown with 100 nm layer of isotopically enriched ^{12}C (99.999%) by plasma-enhanced CVD [63]. The NV center's negative charge state allows optical detection and polarization of its electron spin [64,65]. We apply a bias magnetic field of 490 G parallel to the NV axis to lift the degeneracy of the $m_s = \pm 1$ ground states [Fig. 1(d)] and polarize the nitrogen nuclear spin [66]. We use a 532 nm laser to initialize the system in $|0\rangle$. We prepare a superposition state between $|-1\rangle$ and $|0\rangle$ by a microwave $\pi/2$ pulse, apply a control scheme, and then another $\pi/2$ pulse with a phase that alternates between 0° and 180°, to map coherences back onto populations [Fig. 1(c)]. We estimate the final populations from the difference between the signals, reducing errors due to charge-state and count-rate fluctuations [67]. All control fields originate from the same arbitrary waveform generator and amplifier.

We first consider a Ramsey measurement [33] resulting in a coherence time of $T_2^* = 28.1 \pm 1.8$ μs (estimates are reported ± their standard error throughout the text). Decoupling by one continuous field, resonant with the $|0\rangle \leftrightarrow |-1\rangle$ transition, with $\Omega_1 = (2\pi)4.305$ MHz ± 3 kHz, increases the coherence time to $T_{2\rho,\text{single drive}} = 114.1 \pm 1.3$ μs. We then use standard DD with $\Omega_1 = (2\pi)4.470$ MHz ± 2 kHz and $\Omega_2 = (2\pi)0.896$ MHz ± 2 kHz. We record a sinusoidal trace with frequency Ω_2, which decays with $T_{2\rho,\text{standard DD}} = 256 \pm 8$ μs [see Figs. 2(a), 2(b), and 2(c)]. For correlated DD, we first have to determine c and thus the modulation frequency $\widetilde{\Omega}_1$. We do so by experimentally varying $\widetilde{\Omega}_1$ from Ω_1 to $\Omega_1 + \frac{6}{4}(\Omega_2^2/\Omega_1)$ and measuring the respective coherence times [33]. This specific range is given by Eq. (3) with the $c \to c + \frac{1}{4}$ correction (recalling $|c| \leq 1$). We find that the optimal $\widetilde{\Omega}_1 = (2\pi)4.697$ MHz corresponds to $c \approx 1$ [33], which corroborates our expectation for high noise cross-correlation. The coherence time reaches $T_{2\rho,\text{correlated DD}} \approx 2.8$ ms—an improvement of more than an order of magnitude over standard DD [Fig. 2(a), 2(b) and 2(d)]. It is also 20% higher than the widely used XY8 pulsed dynamical decoupling sequence, which gives 2.32 ms [33]. Given the proximity to the single-drive coherence time limit (cf. $T_{1\rho} \approx 3$ ms [24,68]), it is informative to estimate the relaxation-free coherence time of the two schemes, which demonstrates a greater improvement of 67% [33]. We note that this is achieved without optimizing the Rabi amplitudes, which can further prolong the coherence time [33,69]. In addition, continuous dynamical decoupling has several advantages over pulsed methods, such as uninterrupted protection, negligible memory access latency, and typically lower peak power [70,71].

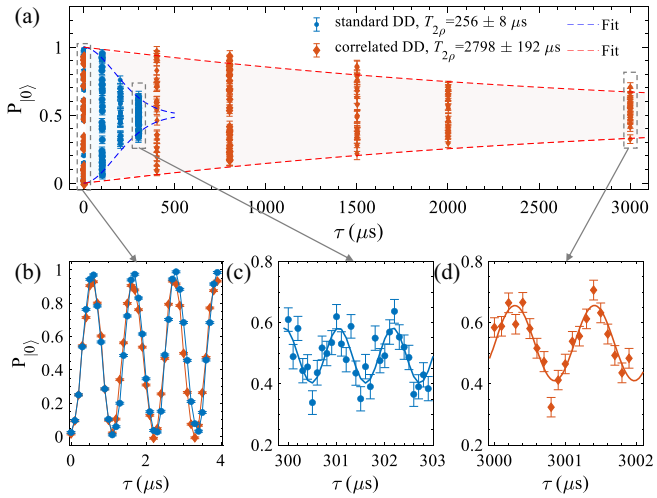

FIG. 2. Experimental measurements of the population of state $|0\rangle$ ($P_{|0\rangle}$) vs experimental time τ, demonstrating improved quantum memory. (a) We fit a stretched exponential function $\exp[-(\tau/T_2)^\beta]$ to the difference between the higher and lower signal envelopes and obtain $T_{2\rho} = 256 \pm 8$ μs ($\beta = 1.86 \pm 0.17$) for standard DD (blue), which is extended twelvefold to $T_{2\rho} = 2.798 \pm 0.192$ ms ($\beta = 1.04 \pm 0.11$) for correlated DD (red). The higher and lower envelope fits are shown with dashed lines. For correlated DD we shift the modulation frequency, $\widetilde{\Omega}_1$, according to Eq. (3) with $c \approx 1$, and the $c \to c + \frac{1}{4}$ correction. (b)–(d) Close-up views of measurements at 1 μs, 300 μs and 3 ms. The frequency of the signal oscillation in the lab frame is $\approx\Omega_2$, as expected from theory.

To further support our findings, we compare standard and correlated DD by a numerical simulation of a qubit subject to environmental noise, typical of NV centers, and correlated field noise, modeled with Ornstein-Uhlenbeck processes [21,33,72–75]. Correlated DD achieves a coherence time of 3.8 ms, an improvement of twenty times over standard DD [33]. The simulation does not account for relaxation and uses lower Rabi frequencies, resulting in longer coherence times and greater improvement than in the experiment, highlighting the potential capabilities of correlated DD. Figure 3 demonstrates the improvement of correlated and standard DD compared to single-drive decoupling for different correlation times of the amplitude noise. Correlated DD outperforms the standard scheme for all correlation times (and corresponding noise spectra), highlighting its broad applicability.

Quantum sensing.—Standard DD has been used for sensing high-frequency (GHz) [22] and low-frequency (sub-MHz) [25] signals with NV centers. The sensitivity, typically limited by photon-shot noise, effective phase accumulation rate, and coherence time [5,22,33,76–78], reads

$$\eta(\tau) = \frac{2}{\gamma_{\text{NV}} \alpha C(\tau) \sqrt{N_{\text{ph}} \tau}}, \tag{4}$$

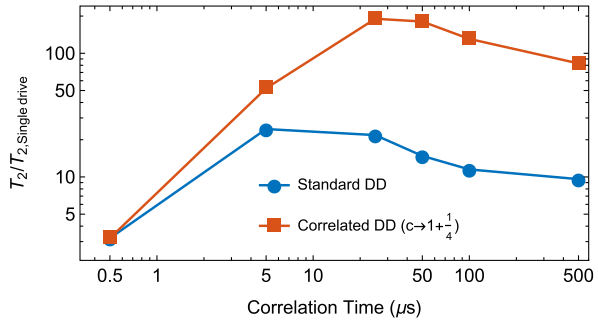

FIG. 3. Simulation of the improvement of coherence time $T_{2\rho}$ for standard and correlated DD in comparison to the single-drive $T_{2\rho} \approx 22.3$ μs for different noise correlation times [33].

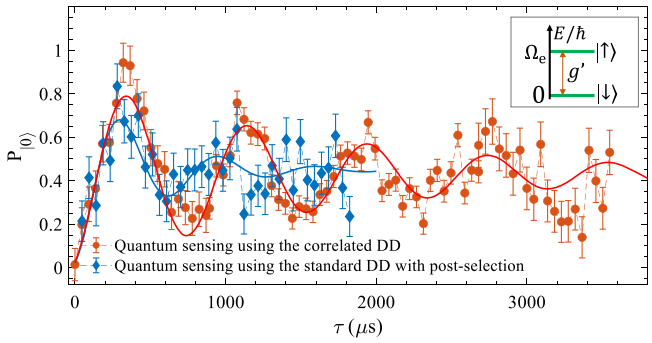

FIG. 4. Quantum sensing measurements of an external high-frequency [$(2\pi)1.487$ GHz] signal of amplitude g_0 using standard and correlated DD with the "low-attenuation" scheme, demonstrating improved sensitivity. We measure the NV state stroboscopically at multiples of $\tau_{\Omega_2} = 2\pi/\Omega_2$, observing Rabi oscillations with angular frequency $g' \approx g_0/2$ in the lab frame. Standard DD's susceptibility to amplitude noise necessitated data postselection. Inset: a schematic of sensing an external signal using the DD protocols.

where the optimal measurement time $\tau \approx T_{2\rho}/2$ [5,33,77], $\gamma_{\text{NV}}/2\pi = 28$ Hz/nT is the gyromagnetic ratio of the NV electron spin, $C(\tau)$ is the signal contrast at time τ [33], and N_{ph} represents the average number of photons per measurement. The attenuation factor α quantifies the effective phase accumulation rate $g' = \alpha g_0$, where g_0 is the amplitude of the sensed field [5,33,79]. One challenge for DD based sensing is this signal attenuation, that is, having a low α.

Previous work [22] has demonstrated sensing of a high-frequency ($\omega_g \sim$ GHz) signal by meeting the resonance condition $\omega_g = \omega_0 - \widetilde{\Omega}_1 - \Omega_e$, where $\Omega_e \equiv \sqrt{\Omega_2^2 + (\Omega_1 - \widetilde{\Omega}_1)^2}$, which has an attenuation factor $\alpha = \frac{1}{4}$. We label this the "high-attenuation" scheme. We demonstrate a "low-attenuation" alternative with $\alpha = \frac{1}{2}$, a twofold improvement in sensitivity, using the resonance condition $\omega_g = \omega_0 - \Omega_e$ [33]. This improvement also confers an advantage for quantum computing schemes that rely on dressed qubits [21].

Figure 4 shows a comparison of standard and correlated DD for quantum sensing. The parameters are $\Omega_1 = (2\pi)4.327$ MHz $\pm$ 3 kHz, $\Omega_2 = (2\pi)0.863$ MHz $\pm$ 2 kHz, and $\widetilde{\Omega}_1 = (2\pi)4.523$ MHz. Standard DD yields a coherence time of $T_{2\rho} = 0.496 \pm 0.142$ ms and an effective signal amplitude of $g' = (2\pi)1.54 \pm 0.11$ kHz. Correlated DD yields $T_{2\rho} = 1.681 \pm 0.288$ ms and $g' = (2\pi)1.251 \pm 0.016$ kHz. We note that $\widetilde{\Omega}_1$ does not include the $c \to (c + \frac{1}{4})$ correction, resulting in slightly lower coherence times than the quantum memory experiments. Standard DD's susceptibility to amplitude noise necessitated data postselection (about 33% was used) to detect signal-induced oscillations, increasing threefold the total measurement time. This was not necessary for correlated DD due to its robustness. We estimate a correlated DD photon-shot noise limited sensitivity of $\eta \approx 13$ nT$/\sqrt{\text{Hz}}$, which is approximately 3.3 times better than with standard DD due to the longer coherence time and less overhead [33]. To our knowledge, this sensitivity is better than the state-of-the-art values for high-frequency (GHz) sensing with a single NV center, which are typically in the range of a few hundred [22,80,81] to several tens of nT$/\sqrt{\text{Hz}}$ [82]. Further refinement in terms of Rabi frequency optimization [24] and photon collection efficiency, can improve sensitivity further.

Robust coherent control.—Coherent control manipulates quantum systems but noise reduces its fidelity. We demonstrate improved robustness to control noise with correlated DD, compared to a conventional π pulse (based on the single drive) and standard DD, in a population transfer simulation in Fig. 5. Note that the speed of operations for each protocol, i.e., the inverse of the pulse duration, is proportional to the effective Rabi frequency of the dressed qubit. Since the amplitude noise scales with the latter, standard DD prolongs the pulse duration and the coherence time by the same factor, compared to the single-drive pulse.

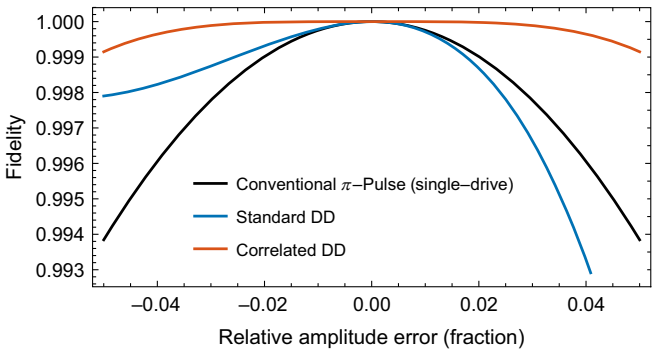

FIG. 5. Simulation of fidelity of population transfer for: conventional π pulse [using a single-drive, black, pulse time $T = (\pi/\Omega_1)$], standard DD [using H_{II} in Eq. (2) and $\widetilde{\Omega}_1 = \Omega_1$, blue, pulse time $= 4T$, $(\Omega_2/\Omega_1) = 0.25$], and correlated DD [using H_{II} in Eq. (2) and $\widetilde{\Omega}_1 = \Omega_1 + (\Omega_2^2/\Omega_1)$, red, pulse time $= 3.75T$, $(\Omega_2/\Omega_1) = (1/\sqrt{15}) \approx 0.258$]. Correlated DD shows superior robustness.

This results in similar robustness for both protocols, as is evident in Fig. 5. On the contrary, correlated DD improves the aforementioned scaling by using destructive interference of errors, which results in better robustness.

Discussion.—Noise cross-correlations emerge naturally in experiments and should be taken into account [33,83]. Examples include amplitude noise and its respective Bloch-Siegert shift, noise in the flux-bias and drive amplitude of a flux qubit [84], and noisy energy shifts and splittings in multilevel systems using multiple control tones [72,85]. Cross-correlations are also present in qubit spatial ensembles addressed by global control fields. Specifically, compensation of amplitude (B_1) inhomogeneity in NV ensembles is feasible with correlated DD. In addition to improving continuous double drive, utilizing cross-correlations can be useful for a wide range of experimental techniques, e.g., for optimization of pulsed decoupling by replacing the standard π pulse with correlated DD (see Fig. 5) and robust coherent control of two- and three-state quantum systems [33]. Furthermore, fluctuations in global operations in ensembles can be addressed using the method presented here, such as the parallel entanglement of Rydberg atoms, as discussed in [86]. Spatiotemporal environmental cross-correlations and cross-talk in coupled multiqubit systems [87–90] also offer possibilities for optimizing multiqubit control by destructive interference of correlated noise.

Conclusion.—In this Letter, we developed and demonstrated experimentally a destructive interference-based noise protection strategy, which relies on the cross-correlation of two noise sources. We achieve an order-of-magnitude extension of coherence times, allowing for longer quantum memories, improved coherent control, and state-of-the-art sensitivity of quantum sensing. Correlated DD expands the range of applicable control amplitudes, since such protocols are typically upper limited by control noise. Implications include higher dynamic range for sensing protocols, faster operations, and improved protection.

The proposed scheme is general and applicable to a wide range of physical systems, including trapped atoms and ions, solid-state defects, and superconducting qubits. Utilizing noise correlations can improve coherent control beyond correlated double drive. Our protocol can be combined with refocusing-based methods. For example, using it within a rotary echo sequence can correct for the slow spectral components of the uncorrelated part of the amplitude noise, if such exists. Composite pulses, pulsed dynamical decoupling, and optimal control can in principle also be optimized with our method when cross-correlated noise is present.

We thank Matthew Markham (Element 6) for the fabrication of the diamond solid immersion lens and Christian Osterkamp (Ulm University) for the growth of the isotopically enriched NV doped layer of CVD diamond. Q. C. is thankful to Raul Gonzalez Cornejo and Gerhard Wolff for experimental help and to Yu Liu for helpful discussions. A. S., A. R., and G. G. thank Nati Aharon for fruitful discussions. A. S. gratefully acknowledges the support of the Clore Israel Foundation Scholars Programme, the Israeli Council for Higher Education, and the Milner Foundation. This work was funded by the German Federal Ministry of Research (BMBF) by future cluster QSENS and projects DE-Brill (No. 13N16207), SPINNING, DIAQNOS (No. 13N16463), quNV2.0 (No. 13N16707), QR. X and Quamapolis (No. 13N15375), DLR via project QUASIMODO (No. 50WM2170), Deutsche Forschungsgemeinschaft (DFG) via Projects No. 386028944, No. 445243414, and No. 387073854, and Excellence Cluster POLiS European Union's HORIZON Europe program via projects QuMicro (No. 101046911), SPINUS (No. 101135699), CQuENS (No. 101135359), QCIRCLE (No. 101059999) and FLORIN (No. 101086142), European Research Council (ERC) via Synergy grant HyperQ (No. 856432) and Carl-Zeiss-Stiftung via the Center of Integrated Quantum Science and technology (IQST) and project Utrasens-Vir. A. R. acknowledges the support of European Research Council grant QRES, Project No. 770929, Quantera grant MfQDS, Israel Science Foundation and the Schwartzmann university chair. J. M. acknowledges the National Natural Science Foundation of China (Grants No. 12161141011).

*alon.salhov@mail.huji.ac.il
†jianmingcai@hust.edu.cn
‡genko.genov@uni-ulm.de
§These authors contributed equally to this work.

[1] W. H. Zurek, Decoherence, einselection, and the quantum origins of the classical, Rev. Mod. Phys. **75**, 715 (2003).
[2] K. Khodjasteh and D. A. Lidar, Fault-tolerant quantum dynamical decoupling, Phys. Rev. Lett. **95**, 180501 (2005).
[3] D. Aharonov and M. Ben-Or, Fault-tolerant quantum computation with constant error, in *Proceedings of the Twenty-Ninth Annual ACM Symposium on Theory of Computing* (ACM, El Paso, 1997), pp. 176–188.
[4] P. W. Shor, Fault-tolerant quantum computation, in *Proceedings of 37th Conference on Foundations of Computer Science* (IEEE, New York, 1996), pp. 56–65.
[5] C. L. Degen, F. Reinhard, and P. Cappellaro, Quantum sensing, Rev. Mod. Phys. **89**, 035002 (2017).
[6] I. Siddiqi, Engineering high-coherence superconducting qubits, Nat. Rev. Mater. **6**, 875 (2021).
[7] B. M. Terhal, Quantum error correction for quantum memories, Rev. Mod. Phys. **87**, 307 (2015).
[8] D. A. Lidar and T. A. Brun, *Quantum Error Correction* (Cambridge University Press, Cambridge, 2013).
[9] D. A. Lidar and K. B. Whaley, Decoherence-free subspaces and subsystems, *Irreversible Quantum Dynamics*, edited by F. Benatti and R. Floreanini, Springer Lecture Notes in Physics (2003), Vol. 622, pp. 83–120, 10.1007/3-540-44874-8_5.

[10] G. Wolfowicz, A. M. Tyryshkin, R. E. George, H. Riemann, N. V. Abrosimov, P. Becker, H.-J. Pohl, M. L. Thewalt, S. A. Lyon, and J. J. Morton, Atomic clock transitions in silicon-based spin qubits, Nat. Nanotechnol. **8**, 561 (2013).
[11] L. Viola, E. Knill, and S. Lloyd, Dynamical decoupling of open quantum systems, Phys. Rev. Lett. **82**, 2417 (1999).
[12] M. H. Levitt, Composite pulses, Prog. Nucl. Magn. Reson. Spectrosc. **18**, 61 (1986).
[13] S. Wimperis, Broadband, narrowband, and passband composite pulses for use in advanced NMR experiments, J. Magn. Reson., Ser. A **109**, 221 (1994).
[14] H. K. Cummins, G. Llewellyn, and J. A. Jones, Tackling systematic errors in quantum logic gates with composite rotations, Phys. Rev. A **67**, 042308 (2003).
[15] B. T. Torosov and N. V. Vitanov, Smooth composite pulses for high-fidelity quantum information processing, Phys. Rev. A **83**, 053420 (2011).
[16] G. T. Genov and N. V. Vitanov, Dynamical suppression of unwanted transitions in multistate quantum systems, Phys. Rev. Lett. **110**, 133002 (2013).
[17] G. T. Genov, D. Schraft, T. Halfmann, and N. V. Vitanov, Correction of arbitrary field errors in population inversion of quantum systems by universal composite pulses, Phys. Rev. Lett. **113**, 043001 (2014).
[18] G. T. Genov, M. Hain, N. V. Vitanov, and T. Halfmann, Universal composite pulses for efficient population inversion with an arbitrary excitation profile, Phys. Rev. A **101**, 013827 (2020).
[19] S. S. Ivanov, B. T. Torosov, and N. V. Vitanov, High-fidelity quantum control by polychromatic pulse trains, Phys. Rev. Lett. **129**, 240505 (2022).
[20] D. Suter and G. A. Álvarez, Colloquium: Protecting quantum information against environmental noise, Rev. Mod. Phys. **88**, 041001 (2016).
[21] J.-M. Cai, B. Naydenov, R. Pfeiffer, L. P. McGuinness, K. D. Jahnke, F. Jelezko, M. B. Plenio, and A. Retzker, Robust dynamical decoupling with concatenated continuous driving, New J. Phys. **14**, 113023 (2012).
[22] A. Stark, N. Aharon, T. Unden, D. Louzon, A. Huck, A. Retzker, U. L. Andersen, and F. Jelezko, Narrow-bandwidth sensing of high-frequency fields with continuous dynamical decoupling, Nat. Commun. **8**, 1105 (2017).
[23] T. Joas, A. M. Waeber, G. Braunbeck, and F. Reinhard, Quantum sensing of weak radio-frequency signals by pulsed Mollow absorption spectroscopy, Nat. Commun. **8**, 964 (2017).
[24] G. Wang, Y.-X. Liu, and P. Cappellaro, Coherence protection and decay mechanism in qubit ensembles under concatenated continuous driving, New J. Phys. **22**, 123045 (2020).
[25] K. Kim, Y. Na, J. Yoon, D. Lee, H. S. Kang, C.-H. Lee, and D. Lee, Sub-MHz ac magnetometry with a double-dressed spin qubit in diamond, arXiv:2207.06611.
[26] A. J. Ramsay, R. Hekmati, C. J. Patrickson, S. Baber, D. R. Arvidsson-Shukur, A. J. Bennett, and I. J. Luxmoore, Coherence protection of spin qubits in hexagonal boron nitride, Nat. Commun. **14**, 461 (2023).
[27] G. Wang, Y.-X. Liu, P. Cappellaro *et al.*, Observation of the high-order Mollow triplet by quantum mode control with concatenated continuous driving, Phys. Rev. A **103**, 022415 (2021).
[28] I. Cohen, N. Aharon, and A. Retzker, Continuous dynamical decoupling utilizing time-dependent detuning, Fortschr. Phys. **65**, 1600071 (2017).
[29] D. Farfurnik, N. Aharon, I. Cohen, Y. Hovav, A. Retzker, and N. Bar-Gill, Experimental realization of time-dependent phase-modulated continuous dynamical decoupling, Phys. Rev. A **96**, 013850 (2017).
[30] J. Teissier, A. Barfuss, and P. Maletinsky, Hybrid continuous dynamical decoupling: A photon-phonon doubly dressed spin, J. Opt. **19**, 044003 (2017).
[31] Q. Y. Cao, P. C. Yang, M. S. Gong, M. Yu, A. Retzker, M. B. Plenio, C. Muller, N. Tomek, B. Naydenov, L. P. McGuinness, F. Jelezko, and J. M. Cai, Protecting quantum spin coherence of nanodiamonds in living cells, Phys. Rev. Appl. **13**, 024021 (2020).
[32] G. T. Genov, N. Aharon, F. Jelezko, and A. Retzker, Mixed dynamical decoupling, Quantum Sci. Technol. **4**, 035010 (2019).
[33] See Supplemental Material at http://link.aps.org/supplemental/10.1103/PhysRevLett.132.223601, which includes Refs. [34–56] and more details on the theory, numerical simulation, additional experimental results, and examples for additional physical scenarios where cross-correlated noise can be utilized.
[34] D. Yudilevich, A. Salhov, I. Schaefer, K. Herb, A. Retzker, and A. Finkler, Coherent manipulation of nuclear spins in the strong driving regime, New J. Phys. **25**, 113042 (2023).
[35] M. D. Bowdrey, D. K. Oi, A. J. Short, K. Banaszek, and J. A. Jones, Fidelity of single qubit maps, Phys. Lett. A **294**, 258 (2002).
[36] B. A. Myers, A. Ariyaratne, and A. C. Bleszynski Jayich, Double-quantum spin-relaxation limits to coherence of near-surface nitrogen-vacancy centers, Phys. Rev. Lett. **118**, 197201 (2017).
[37] M. C. Cambria, A. Gardill, Y. Li, A. Norambuena, J. R. Maze, and S. Kolkowitz, State-dependent phonon-limited spin relaxation of nitrogen-vacancy centers, Phys. Rev. Res. **3**, 013123 (2021).
[38] M. Loretz, T. Rosskopf, and C. L. Degen, Radio-frequency magnetometry using a single electron spin, Phys. Rev. Lett. **110**, 017602 (2013).
[39] H. Y. Carr and E. M. Purcell, Effects of diffusion on free precession in nuclear magnetic resonance experiments, Phys. Rev. **94**, 630 (1954).
[40] S. Meiboom and D. Gill, Modified spin-echo method for measuring nuclear relaxation times, Rev. Sci. Instrum. **29**, 688 (1958).
[41] G. E. Santyr, R. M. Henkelman, and M. J. Bronskill, Variation in measured transverse relaxation in tissue resulting from spin locking with the CPMG sequence, J. Magn. Reson. **79**, 28 (1988).
[42] N. Bar-Gill, L. M. Pham, A. Jarmola, D. Budker, and R. L. Walsworth, Solid-state electronic spin coherence time approaching one second, Nat. Commun. **4**, 1743 (2013).
[43] M. Steiner, P. Neumann, J. Beck, F. Jelezko, and J. Wrachtrup, Universal enhancement of the optical readout fidelity of single electron spins at nitrogen-vacancy centers in diamond, Phys. Rev. B **81**, 035205 (2010).

[44] F. K. Wilhelm, S. Kirchhoff, S. Machnes, N. Wittler, and D. Sugny, An introduction into optimal control for quantum technologies, arXiv:2003.10132.
[45] B. W. Shore, *The Theory of Coherent Atomic Excitation* (Wiley, New York, 1990).
[46] B. Shore, *Manipulating Quantum Structures Using Laser Pulses* (Cambridge University Press, Cambridge, 2011).
[47] R. P. Feynman, F. L. Vernon, Jr., and R. W. Hellwarth, Geometrical representation of the Schrödinger equation for solving Maser problems, J. Appl. Phys. **28**, 49 (1957).
[48] N. V. Vitanov and S. Stenholm, Analytic properties and effective two-level problems in stimulated Raman adiabatic passage, Phys. Rev. A **55**, 648 (1997).
[49] N. V. Vitanov and B. W. Shore, Stimulated Raman adiabatic passage in a two-state system, Phys. Rev. A **73**, 053402 (2006).
[50] B. T. Torosov and N. V. Vitanov, Composite stimulated Raman adiabatic passage, Phys. Rev. A **87**, 043418 (2013).
[51] C. J. Foot, *Atomic Physics* (Oxford University Press, New York, 2005), Chap. 7.
[52] A. Bruns, G. T. Genov, M. Hain, N. V. Vitanov, and T. Halfmann, Experimental demonstration of composite stimulated Raman adiabatic passage, Phys. Rev. A **98**, 053413 (2018).
[53] T. R. Eichhorn *et al.*, Hyperpolarized solution-state NMR spectroscopy with optically polarized crystals, J. Am. Chem. Soc. **144**, 2511 (2022).
[54] A. Marshall, A. Salhov, M. Gierse, C. Müller, M. Keim, S. Lucas, A. Parker, J. Scheuer, C. Vassiliou, P. Neumann, F. Jelezko, A. Retzker, J. W. Blanchard, I. Schwartz, and S. Knecht, Radio-frequency sweeps at microtesla fields for parahydrogen-induced polarization of biomolecules, J. Phys. Chem. Lett. **14**, 2125 (2023).
[55] M. C. Korzeczek, L. Dagys, C. Müller, B. Tratzmiller, A. Salhov, T. Eichhorn, J. Scheuer, S. Knecht, M. B. Plenio, and I. Schwartz, Towards a unified picture of polarization transfer—Pulsed DNP and chemically equivalent PHIP, J. Magn. Reson. **362**, 107671 (2024).
[56] G. T. Genov, D. Schraft, N. V. Vitanov, and T. Halfmann, Arbitrarily accurate pulse sequences for robust dynamical decoupling, Phys. Rev. Lett. **118**, 133202 (2017).
[57] F. Kong, P. Zhao, X. Ye, Z. Wang, Z. Qin, P. Yu, J. Su, F. Shi, and J. Du, Nanoscale zero-field electron spin resonance spectroscopy, Nat. Commun. **9**, 1563 (2018).
[58] C. Cohen-Tannoudji, *Atoms in Electromagnetic Fields* (World Scientific, Singapore, 1994), Vol. 1.
[59] F. Bloch and A. Siegert, Magnetic resonance for nonrotating fields, Phys. Rev. **57**, 522 (1940).
[60] D. James and J. Jerke, Effective Hamiltonian theory and its applications in quantum information, Can. J. Phys. **85**, 625 (2007).
[61] J. Hadden, J. Harrison, A. C. Stanley-Clarke, L. Marseglia, Y.-L. Ho, B. Patton, J. L. O'Brien, and J. Rarity, Strongly enhanced photon collection from diamond defect centers under microfabricated integrated solid immersion lenses, Appl. Phys. Lett. **97**, 241901 (2010).
[62] P. Siyushev, F. Kaiser, V. Jacques, I. Gerhardt, S. Bischof, H. Fedder, J. Dodson, M. Markham, D. Twitchen, F. Jelezko *et al.*, Monolithic diamond optics for single photon detection, Appl. Phys. Lett. **97**, 241902 (2010).
[63] C. Osterkamp, J. Lang, J. Scharpf, C. Müller, L. P. McGuinness, T. Diemant, R. J. Behm, B. Naydenov, and F. Jelezko, Stabilizing shallow color centers in diamond created by nitrogen delta-doping using SF_6 plasma treatment, Appl. Phys. Lett. **106**, 113109 (2015).
[64] N. B. Manson, J. P. Harrison, and M. J. Sellars, Nitrogen-vacancy center in diamond: Model of the electronic structure and associated dynamics, Phys. Rev. B **74**, 104303 (2006).
[65] M. W. Doherty, N. B. Manson, P. Delaney, F. Jelezko, J. Wrachtrup, and L. C. Hollenberg, The nitrogen-vacancy colour centre in diamond, Phys. Rep. **528**, 1 (2013).
[66] V. Jacques, P. Neumann, J. Beck, M. Markham, D. Twitchen, J. Meijer, F. Kaiser, G. Balasubramanian, F. Jelezko, and J. Wrachtrup, Dynamic polarization of single nuclear spins by optical pumping of nitrogen-vacancy color centers in diamond at room temperature, Phys. Rev. Lett. **102**, 057403 (2009).
[67] T. Häberle, T. Oeckinghaus, D. Schmid-Lorch, M. Pfender, F. F. de Oliveira, S. A. Momenzadeh, A. Finkler, and J. Wrachtrup, Nuclear quantum-assisted magnetometer, Rev. Sci. Instrum. **88**, 013702 (2017).
[68] P. Krantz, M. Kjaergaard, F. Yan, T. P. Orlando, S. Gustavsson, and W. D. Oliver, A quantum engineer's guide to superconducting qubits, Appl. Phys. Rev. **6**, 021318 (2019).
[69] N. Ezzell, B. Pokharel, L. Tewala, G. Quiroz, and D. A. Lidar, Dynamical decoupling for superconducting qubits: A performance survey, Phys. Rev. Appl. **20**, 064027 (2023).
[70] K. Khodjasteh, J. Sastrawan, D. Hayes, T. J. Green, M. J. Biercuk, and L. Viola, Designing a practical high-fidelity long-time quantum memory, Nat. Commun. **4**, 2045 (2013).
[71] K. C. Miao, J. P. Blanton, C. P. Anderson, A. Bourassa, A. L. Crook, G. Wolfowicz, H. Abe, T. Ohshima, and D. D. Awschalom, Universal coherence protection in a solid-state spin qubit, Science **369**, 1493 (2020).
[72] N. Aharon, I. Cohen, F. Jelezko, and A. Retzker, Fully robust qubit in atomic and molecular three-level systems, New J. Phys. **18**, 123012 (2016).
[73] M. C. Wang and G. E. Uhlenbeck, On the theory of the Brownian motion II, Rev. Mod. Phys. **17**, 323 (1945).
[74] D. T. Gillespie, Exact numerical simulation of the Ornstein-Uhlenbeck process and its integral, Phys. Rev. E **54**, 2084 (1996).
[75] D. T. Gillespie, The mathematics of Brownian motion and Johnson noise, Am. J. Phys. **64**, 225 (1996).
[76] J. M. Taylor, P. Cappellaro, L. Childress, L. Jiang, D. Budker, P. Hemmer, A. Yacoby, R. Walsworth, and M. Lukin, High-sensitivity diamond magnetometer with nanoscale resolution, Nat. Phys. **4**, 810 (2008).
[77] J. F. Barry, J. M. Schloss, E. Bauch, M. J. Turner, C. A. Hart, L. M. Pham, and R. L. Walsworth, Sensitivity optimization for NV-diamond magnetometry, Rev. Mod. Phys. **92**, 015004 (2020).
[78] L. Rondin, J.-P. Tetienne, T. Hingant, J.-F. Roch, P. Maletinsky, and V. Jacques, Magnetometry with nitrogen-vacancy defects in diamond, Rep. Prog. Phys. **77**, 056503 (2014).

[79] G. Wang, Y.-X. Liu, Y. Zhu, and P. Cappellaro, Nanoscale vector ac magnetometry with a single nitrogen-vacancy center in diamond, Nano Lett. **21**, 5143 (2021).
[80] J. Meinel, V. Vorobyov, B. Yavkin, D. Dasari, H. Sumiya, S. Onoda, J. Isoya, and J. Wrachtrup, Heterodyne sensing of microwaves with a quantum sensor, Nat. Commun. **12**, 2737 (2021).
[81] P. Wang, Z. Yuan, P. Huang, X. Rong, M. Wang, X. Xu, C. Duan, C. Ju, F. Shi, and J. Du, High-resolution vector microwave magnetometry based on solid-state spins in diamond, Nat. Commun. **6**, 6631 (2015).
[82] N. Staudenmaier, S. Schmitt, L. P. McGuinness, and F. Jelezko, Phase-sensitive quantum spectroscopy with high-frequency resolution, Phys. Rev. A **104**, L020602 (2021).
[83] I. Almog, G. Loewenthal, J. Coslovsky, Y. Sagi, and N. Davidson, Dynamic decoupling in the presence of colored control noise, Phys. Rev. A **94**, 042317 (2016).
[84] F. Yan, S. Gustavsson, J. Bylander, X. Jin, F. Yoshihara, D. G. Cory, Y. Nakamura, T. P. Orlando, and W. D. Oliver, Rotating-frame relaxation as a noise spectrum analyser of a superconducting qubit undergoing driven evolution, Nat. Commun. **4**, 2337 (2013).
[85] I. V. Zalivako, A. S. Borisenko, I. A. Semerikov, A. E. Korolkov, P. L. Sidorov, K. P. Galstyan, N. V. Semenin, V. N. Smirnov, M. D. Aksenov, A. K. Fedorov, K. Y. Khabarova, and N. N. Kolachevsky, Continuous dynamical decoupling of optical $^{171}Yb^{+}$ qudits with radiofrequency fields, Front. Quantum Sci. Technol. **2**, 1228208 (2023).
[86] D. Bluvstein, S. J. Evered, A. A. Geim, S. H. Li, H. Zhou, T. Manovitz, S. Ebadi, M. Cain, M. Kalinowski, D. Hangleiter *et al.*, Logical quantum processor based on reconfigurable atom arrays, Nature (London) **626**, 58 (2023).
[87] U. von Lüpke, F. Beaudoin, L. M. Norris, Y. Sung, R. Winik, J. Y. Qiu, M. Kjaergaard, D. Kim, J. Yoder, S. Gustavsson *et al.*, Two-qubit spectroscopy of spatiotemporally correlated quantum noise in superconducting qubits, PRX Quantum **1**, 010305 (2020).
[88] C. E. Bradley, J. Randall, M. H. Abobeih, R. C. Berrevoets, M. J. Degen, M. A. Bakker, M. Markham, D. J. Twitchen, and T. H. Taminiau, A ten-qubit solid-state spin register with quantum memory up to one minute, Phys. Rev. X **9**, 031045 (2019).
[89] D. L. Mickelsen, H. M. Carruzzo, and C. C. Yu, Interacting two-level systems as a source of $1/f$ charge noise in quantum dot qubits, Phys. Rev. B **108**, 195307 (2023).
[90] R. Harper and S. T. Flammia, Learning correlated noise in a 39-qubit quantum processor, PRX Quantum **4**, 040311 (2023).